Mixed-Port Scattering and Hybrid Parameters for High-Speed Differential Lines

Arif Ege Engin, *Member, IEEE*, Ivan Ndip, *Senior Member, IEEE*, Klaus-Dieter Lang, *Senior Member, IEEE*, and Gerardo Aguirre, *Senior Member, IEEE*

***Abstract*—High-speed transmission lines are commonly routed as differential lines to control sensitivity to noise on the reference planes at higher speeds. Differential lines are typically characterized in terms of mixed-mode scattering parameters, as they provide insight into the behavior of differential and common signals, as well as the mode conversion among them. These mixed-mode scattering parameters can be mathematically obtained from single-ended parameters, which can, for example, be measured with a four-port vector network analyzer. There has been recent efforts to develop extended or modified versions of mixed-mode scattering parameters, especially for tightly-coupled lines. This can be a point of confusion in interpreting the behavior of differential lines. In this paper, we introduce the mixed-port scattering and hybrid parameters, which do not suffer from any such ambiguous definitions. Mixed-port hybrid parameters are the most natural way to represent any four-port differential circuit, as they are based on intuitive differential and common-port excitations of the network. They also enable extraction of the current division factor experimentally, which is a critical parameter for electromagnetic interference analysis of differential lines. Mixed-port scattering parameters are also defined based on common and differential port excitations, allowing a simpler interpretation than their mixed-mode counterparts, without the need for defining even, odd, common, or differential-mode impedances. As such, mixed-port scattering and hybrid parameters can be used to analyze the performance of a general differential network, certainly including coupled or asymmetrical lines, without any ambiguity.**

***Index Terms*—Current division factor, differential lines, mixed-mode scattering parameters, mode conversion.**

I. Introduction

SINGLE-ENDED to mixed-mode conversion can be considered as a linear transformation of nodal voltages and currents into modal ones, by assigning a differential and common-mode voltage and current to each port pair. For the more commonly used mixed-mode scattering parameters, the transformation is from single-ended power waves into differential and common-mode power waves [1]. These linear transformations can be done with arbitrary coefficients, resulting in various definitions of mixed-mode parameters [2]–[4]. Mixed-mode parameters have also been defined for the impedance and admittance matrices [5], chain scattering parameters [6], as well as ABCD parameters [7]. A major advantage of working with mixed-mode parameters is that they allow to gain intuition into the properties of a differential network with a quick glance.

In this paper, we introduce *mixed-port* scattering and hybrid parameters, which provide an intuitive view into the definition of differential and common signals, while not suffering from ambiguities existing in earlier *mixed-mode* parameters. The new mixed-port parameters introduced in this paper are based on the common- and differential-port excitations as shown in Fig. 1. The mixed-port parameters obtained with such measurement ports will be referenced to the actual port impedances, without requiring the definition of even, odd, common, or differential-mode impedances.

Fig. 2(a) shows a pair of single-ended ports in a general microwave network. The traditional mixed-mode scattering parameters are calculated based on common-mode and

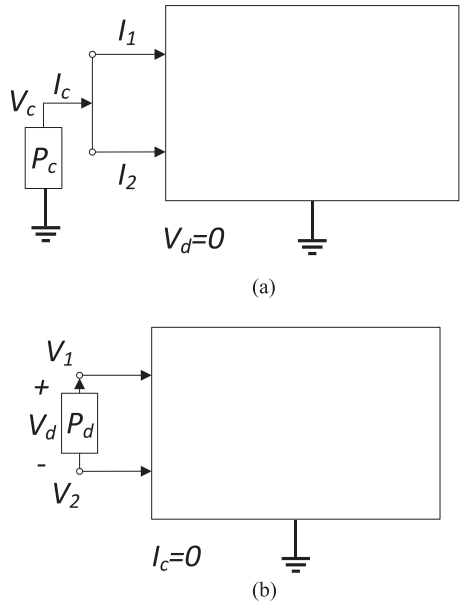

Fig. 1. New port definitions. (a) Common port (P_c). (b) Differential port (P_d).

Manuscript received April 10, 2018; revised May 10, 2018 and June 11, 2018; accepted July 9, 2018. This work was supported in part by the National Science Foundation under Grant No. 1408637 and in part by Alexander von Humboldt Foundation. *(Corresponding author: Arif Ege Engin.)*

A. E. Engin is with the Department of Electrical and Computer Engineering, San Diego State University, San Diego, CA 92182 USA (e-mail: aengin@mail.sdsu.edu).

I. Ndip and K.-D. Lang are with the Fraunhofer-Institut fuer Zuverlaessigkeit und Mikrointegration IZM, Berlin 82234, Germany (e-mail: ivan.ndip@izm.fraunhofer.de; klaus-dieter.lang@izm.fraunhofer.de).

J. Aguirre is with the Kyocera North America, San Diego, CA 92111 USA (e-mail: Jerry.Aguirre@kyocera.com).

Color versions of one or more of the figures in this paper are available online at http://ieeexplore.ieee.org.

Digital Object Identifier 10.1109/TEMC.2018.2855040

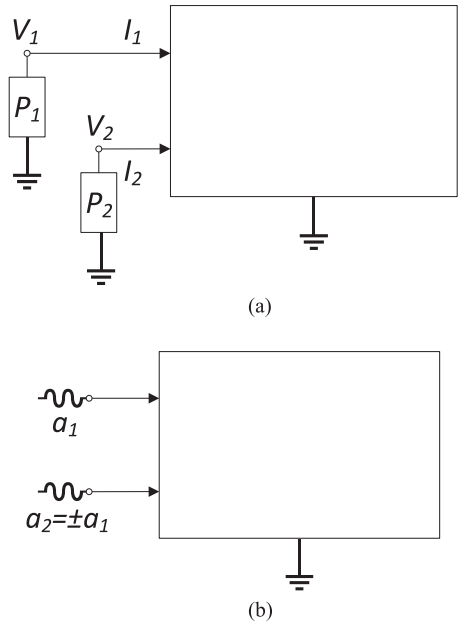

Fig. 2. Traditional port definitions for single-ended and mixed-mode excitation. (a) Single-ended pair of ports (P_1 and P_2). (b) Mixed-mode excitation by common ($a_2 = a_1$) or differential ($a_2 = -a_1$) mode power waves [1].

differential-mode power waves [1] as shown in Fig. 2(b). Such a measurement requires exciting both single-ended ports in-phase and with a 180° phase shift, which can, for example, be accomplished by using a balun. We eliminate the need for such phase alignments in the proposed mixed-port parameters.

To develop the intuitive nature of the mixed-port hybrid parameters, we start by defining possible port excitations for the differential and common signals. This allows us to relate the developed parameters to a possible simulation or measurement setup. The common port is across the shorted single-ended ports and ground reference as shown in Fig. 1(a). We define the differential port across the two single-ended ports as shown in Fig. 1(b). An advantage of such a mixed-port definition is that these ports can be realized in electromagnetic simulators (e.g., differential and common-mode ports in Sonnet [8]), and implemented on test boards similar to single-ended ports. Therefore, we define the ports in a more intuitive way as physical ports, as opposed to based on modes in traditional mixed-mode parameters. This eliminates the ambiguity in defining unequal even- and odd-mode impedances depending on the coupling level in differential lines [2], [9], [10]. In [11] and [12], we introduce the mixed-port hybrid and scattering parameters, respectively. In this paper, we present a comprehensive derivation of these parameters and their relation to each other. We also introduce a methodology to extract the current division factor experimentally; and provide simulation to hardware correlation. The advantages of these new mixed-port scattering and hybrid parameters over existing mixed-mode definitions can be summarized as follows.

1) The mixed-port hybrid parameters allow experimental characterization of the current division factor, which is a critical parameter to assess the behavior of differential lines for electromagnetic interference.
2) The mixed-port scattering parameters can be characterized with simple two-port measurement or simulation setups for the differential ports, common ports, or a combination of them. The reference impedance of such scattering parameters is unambiguously defined from the port impedances.

II. Mixed-Port Hybrid Parameters

A. Modal Voltages and Currents

The traditional definition of differential and common-mode voltages and currents are

$$\begin{pmatrix} V_d \\ V_c \end{pmatrix} = \begin{pmatrix} 1 & -1 \\ 1/2 & 1/2 \end{pmatrix} \begin{pmatrix} V_1 \\ V_2 \end{pmatrix} \tag{1}$$

and

$$\begin{pmatrix} I_d \\ I_c \end{pmatrix} = \begin{pmatrix} 1/2 & -1/2 \\ 1 & 1 \end{pmatrix} \begin{pmatrix} I_1 \\ I_2 \end{pmatrix} \tag{2}$$

where the subscripts 1 and 2 represent the pair of single-ended ports. From these modal voltages and currents, differential and common-mode power waves can also be defined, which result in mixed-mode scattering parameters. In contrast, mixed-port hybrid parameters relate voltages and currents rather than power waves. Specifically, the common current is excited by defining a port across the shorted single-ended ports and ground reference, which results in $V_d = V_1 - V_2 = 0$, as shown in Fig. 1(a). We excite the differential voltage by defining a port across the two single-ended ports as in Fig. 1(b). This differential excitation results in $I_c = I_1 + I_2 = 0$. As a result, we obtain a straightforward way to enforce either I_c or V_d to zero, which results in mixed-port hybrid parameters.

B. Four-Port Networks

An important special case is when the network is a four-port, such as in a differential line. We define the mixed-port hybrid parameters in this case as

$$\left[\begin{array}{c} I_{d1} \\ I_{d2} \\ \hline V_{c1} \\ V_{c2} \end{array}\right] = \left[\begin{array}{cc|cc} G_{dd11} & G_{dd12} & G_{dc11} & G_{dc12} \\ G_{dd21} & G_{dd22} & G_{dc21} & G_{dc22} \\ \hline G_{cd11} & G_{cd12} & G_{cc11} & G_{cc12} \\ G_{cd21} & G_{cd22} & G_{cc21} & G_{cc22} \end{array}\right] \left[\begin{array}{c} V_{d1} \\ V_{d2} \\ \hline I_{c1} \\ I_{c2} \end{array}\right] \tag{3}$$

or in more compact form using submatrices as

$$\left[\begin{array}{c} I_d \\ \hline V_c \end{array}\right] = \left[\begin{array}{c|c} G_{dd} & G_{dc} \\ \hline G_{cd} & G_{cc} \end{array}\right] \left[\begin{array}{c} V_d \\ \hline I_c \end{array}\right]. \tag{4}$$

Since we can enforce I_c or V_d terms on the right-hand side to be equal to zero by differential and common-port excitations, the mixed-port hybrid parameters present a new intuitive approach for characterization of differential networks. The submatrices along the diagonal (G_{dd} and G_{cc} terms) can be calculated by two separate two-port measurements as shown in Fig. 3. The port configuration in Fig. 3(a) provides the elements of the G_{cc} matrix as $V_{d1} = V_{d2} = 0$ with the common-port excitation on

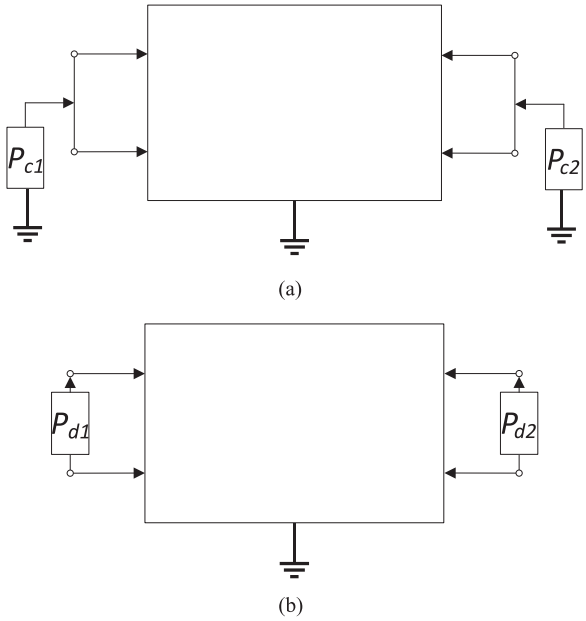

Fig. 3. Two-port excitation of a four-port network to extract. (a) Common. (b) Differential-port parameters.

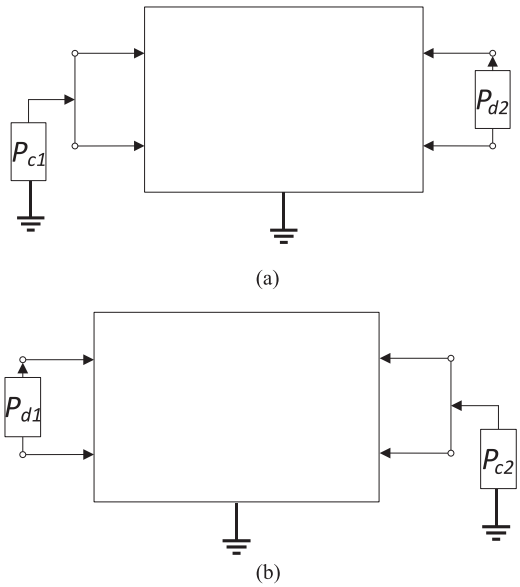

Fig. 4. Two-port excitation of a four-port network to characterize mode conversion.

both sides. From the port configuration in Fig. 3(b), we can extract the elements of G_{dd}.

Mode conversion can be characterized using the mixed-port excitations in Fig. 4. From Fig. 4(a), we can extract

$$\begin{bmatrix} G_{dd22} & G_{dc21} \\ G_{cd12} & G_{cc11} \end{bmatrix}. \tag{5}$$

Finally, from the port configuration in Fig. 4(b), we obtain

$$\begin{bmatrix} G_{dd11} & G_{dc12} \\ G_{cd21} & G_{cc22} \end{bmatrix}. \tag{6}$$

Some redundancy in these measurements can be observed. As a result, not every element of the hybrid mixed-mode parameters can be characterized with this measurement setup. Specifically, $G_{dc11}, G_{dc22}, G_{cd11}, G_{cd22}$ parameters cannot be characterized with these four measurements.

Obtaining all the elements of mixed-port hybrid parameters would require additional measurements or simulations. One approach to obtain the full matrix would be conversion from other mixed-mode representations. For example, if the mixed-mode impedance matrix is given as

$$\left[\begin{array}{c} V_d \\ \hline V_c \end{array}\right] = \left[\begin{array}{c|c} Z_{dd} & Z_{dc} \\ \hline Z_{cd} & Z_{cc} \end{array}\right] \left[\begin{array}{c} I_d \\ \hline I_c \end{array}\right] \tag{7}$$

the hybrid parameters can be obtained as

$$\left[\begin{array}{c} I_d \\ \hline V_c \end{array}\right] = \left[\begin{array}{c|c} Z_{dd}^{-1} & -Z_{dd}^{-1}Z_{dc} \\ \hline Z_{cd}Z_{dd}^{-1} & Z_{cc} - Z_{cd}Z_{dd}^{-1}Z_{dc} \end{array}\right] \left[\begin{array}{c} V_d \\ \hline I_c \end{array}\right]. \tag{8}$$

Single-ended impedance parameters, given by $V = ZI$, can also be directly converted to mixed-port hybrid parameters as

$$G = \frac{1}{2}(M_1 Z + M_2)(M_2 Z + M_1)^{-1} \tag{9}$$

based on the transformation matrices M_1 and M_2 defined as

$$M_1 = \begin{bmatrix} 0 & 0 & 0 & 0 \\ 0 & 0 & 0 & 0 \\ 1 & 1 & 0 & 0 \\ 0 & 0 & 1 & 1 \end{bmatrix} \tag{10}$$

$$M_2 = \begin{bmatrix} 1 & -1 & 0 & 0 \\ 0 & 0 & 1 & -1 \\ 0 & 0 & 0 & 0 \\ 0 & 0 & 0 & 0 \end{bmatrix} \tag{11}$$

which transform single-ended ports to mixed ports

$$\left[\begin{array}{c} I_d \\ \hline V_c \end{array}\right] = \frac{1}{2}M_1 V + \frac{1}{2}M_2 I \tag{12}$$

$$\left[\begin{array}{c} V_d \\ \hline I_c \end{array}\right] = M_2 V + M_1 I. \tag{13}$$

The mixed-port hybrid matrix can also be completely characterized without conversion from other parameters. This is based on additional two-port measurements to fill in the missing four terms as it will be described in Section II-C.

C. Characterization of Current Division Factor

An important special case to consider is asymmetrical transmission lines. Traditional mixed-mode scattering parameters will exhibit mode conversion for this case. An extended mixed-mode scattering matrix is defined in [2], which results in no mode-conversion by making use of a current division factor to perform the modal transformations. The new differential-port parameters in this paper will be the same as the extended parameters for such asymmetrical transmission lines. An advantage of the new differential-port parameters is that it does not require

a prior calculation of the current division factor. As such, it retains the simplicity of the traditional mixed-mode scattering parameters.

The current division factor h in [2], [13] is calculated from the transmission line inductance or capacitance matrix. In this paper, we introduce a measurement based characterization of h. This parameter can be extracted from G_{dc11} for the left side, or G_{dc22} for the right side. For the example of left side, G_{dc11} is defined as

$$G_{dc11} = \frac{I_{d1}}{I_{c1}} = \frac{1}{2}\frac{I_1 - I_2}{I_1 + I_2}. \tag{14}$$

The current division factor is defined as the ratio of the current in port 1 to the total common-mode current. Based on the common port excitation in Fig. 1(a), h can be calculated as

$$\begin{aligned} h &= \frac{I_1}{I_{c1}} = \frac{I_1}{I_1 + I_2} = \frac{1}{2}\left(1 + \frac{I_1 - I_2}{I_1 + I_2}\right) \\ &= \frac{1}{2}(1 + 2G_{dc11}) = \frac{1}{2} + G_{dc11}. \end{aligned} \tag{15}$$

Unlike the transmission-line approach in [2], this current division factor is not limited to differential lines and can be calculated for an arbitrary microwave network. The current division factor can be different for the left and right sides on the network. Equivalent voltage division factors can also be defined based on G_{cd11} and G_{cd22} parameters. For the example of the left side of the network, we define the voltage division factor as the ratio of the negative of the voltage in port 2 to the differential-port voltage, which can be obtained as

$$h = \frac{-V_2}{V_1 - V_2} = \frac{1}{2}\left(1 - \frac{V_1 + V_2}{V_1 - V_2}\right) = \frac{1}{2}(1 - 2G_{cd11}) = \frac{1}{2} - G_{cd11}. \tag{16}$$

Both h factors in (15) and (16) are equivalent (i.e., $G_{dc11} = -G_{cd11}$) for reciprocal networks. To prove that, consider the single-ended excitation of the two-ports on the left side of the network as shown in Fig. 2(a). Enforcing the differential voltage and common current to zero on the right side of the network would require short circuiting the two right ports together, which is not shown in the figure. Assume now that the impedance matrix for the two ports on the left side of the network is obtained as

$$\begin{bmatrix} V_1 \\ V_2 \end{bmatrix} = \begin{bmatrix} Z_{11} & Z_{12} \\ Z_{21} & Z_{22} \end{bmatrix} \begin{bmatrix} I_1 \\ I_2 \end{bmatrix}. \tag{17}$$

This single-ended impedance matrix can be used to calculate the current and voltage division factors. The current division factor is defined when there is a common-port excitation, or $V_1 = V_2$. Enforcing this condition on the single-ended impedance matrix results in

$$Z_{11}I_1 + Z_{12}I_2 = Z_{21}I_1 + Z_{22}I_2 \tag{18}$$

which yields the current division factor in (15) as

$$h = \frac{I_1}{I_1 + I_2} = \frac{Z_{22} - Z_{12}}{Z_{11} - Z_{12} - Z_{21} + Z_{22}}. \tag{19}$$

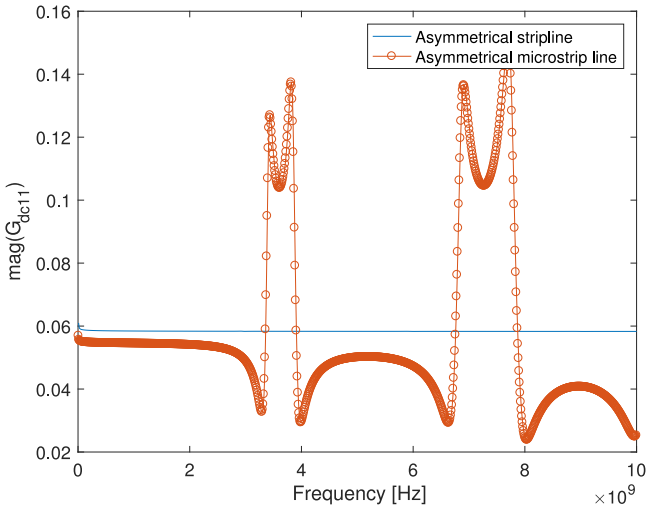

Fig. 5. $G_{dc11} = I_{d1}/I_{c1}$ represents the ratio of differential current to common current. Asymmetrical microstrip lines result in strong-frequency dependent variation due to the presence of inhomogeneous medium.

In a similar way, the voltage division factor in (16) is obtained when there is a differential-port excitation, or $I_1 = -I_2$. Enforcing this condition results in

$$V_1 = (Z_{11} - Z_{12})I_1 \tag{20}$$

$$V_2 = (Z_{21} - Z_{22})I_1 \tag{21}$$

which yields the voltage division factor in (16) as

$$h = \frac{-V_2}{V_1 - V_2} = \frac{Z_{22} - Z_{21}}{Z_{11} - Z_{12} - Z_{21} + Z_{22}}. \tag{22}$$

This shows that the current and voltage division factors are equivalent for any reciprocal network. Based on these additional single-ended two-port measurements, current or voltage division factors can therefore be calculated to obtain the remaining four elements G_{dc11}, G_{dc22}, G_{cd11}, G_{cd22}.

Current or voltage division factors can vary as a function of frequency for asymmetrical transmission lines in an inhomogeneous medium (e.g., microstrip lines), as the transformation matrices given in [2] do not diagonalize the inductance and capacitance matrices simultaneously for the case of inhomogeneous medium [14]. As an example, a 1-in long coupled microstrip line is simulated using Keysight ADS [15], on a substrate with a thickness of 100 μm, dielectric constant of 4, and loss tangent of 0.025. The conductors are 1 oz. copper, with a spacing of 100 μm between line 1 and line 2, which have a width of 150 μm and 100 μm, respectively. Another simulation was done by covering the microstrip lines with another 100 μm-thick substrate and a ground plane to obtain a coupled stripline configuration. Fig. 5 shows the variation of G_{dc11} as a function of frequency. A constant current division factor h, or G_{dc11}, is obtained for the stripline case. The microtrip line, on the other hand, has strong-frequency dependent variation due to the presence of inhomogeneous medium. As a result, the extended mixed-mode parameters in [2] would not decouple the differential and common modes in this case.

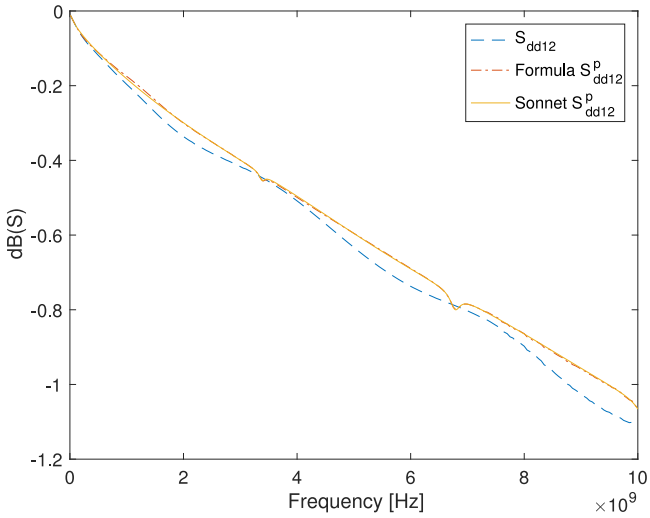

Fig. 6. Traditional differential-mode scattering parameters (S_{dd}) can be different than new differential-port scattering parameters (S_{dd}^{p}) for asymmetrical lines. The Sonnet simulation setup corresponds to the differential-port setup in Fig. 3(b); therefore, it matches the calculated S_{dd}^{p} from the formula in (24).

III. Mixed-Port Scattering Parameters

For high speed or microwave networks, the measurement setups in Figs. 3 and 4 can be used to characterize the scattering parameters. These scattering parameters are different than the traditional mixed-mode scattering parameters. For example, the differential-port scattering parameters in Fig. 3(b) are obtained under the condition that the common port is left unterminated. Some differential signal interface standards such as low-voltage differential signaling (LVDS) indeed specify a single-resistor (differential) termination [16], [17]. In addition, eye diagrams of differential lines are occasionally generated with a solely differential termination [18], [19]. The new mixed-port scattering parameters would be a more intuitive definition of scattering parameters in such cases where only the differential mode is terminated. In contrast, traditional differential-mode scattering parameters assume that there is a termination of common-mode signals as well.

The traditional mixed-mode scattering parameters are given as

$$\begin{bmatrix} b_d \\ \hline b_c \end{bmatrix} = \left[\begin{array}{c|c} S_{dd} & S_{dc} \\ \hline S_{cd} & S_{cc} \end{array}\right] \begin{bmatrix} a_d \\ \hline a_c \end{bmatrix} \tag{23}$$

where S_{dd} is a 2×2 matrix representing the differential-mode scattering parameters. The conversion from the traditional mixed-mode (S_{dd}) to new differential-port scattering parameters (S_{dd}^{p}) can then obtained by assigning $I_c = 0$ or $b_c = a_c$ as

$$S_{dd}^{p} = S_{dd} + S_{dc}\left(1 - S_{cc}\right)^{-1} S_{cd} \tag{24}$$

where S_{dd}^{p} is a 2×2 matrix with elements given as

$$S_{dd}^{p} = \begin{bmatrix} S_{dd11}^{p} & S_{dd12}^{p} \\ S_{dd21}^{p} & S_{dd22}^{p} \end{bmatrix}. \tag{25}$$

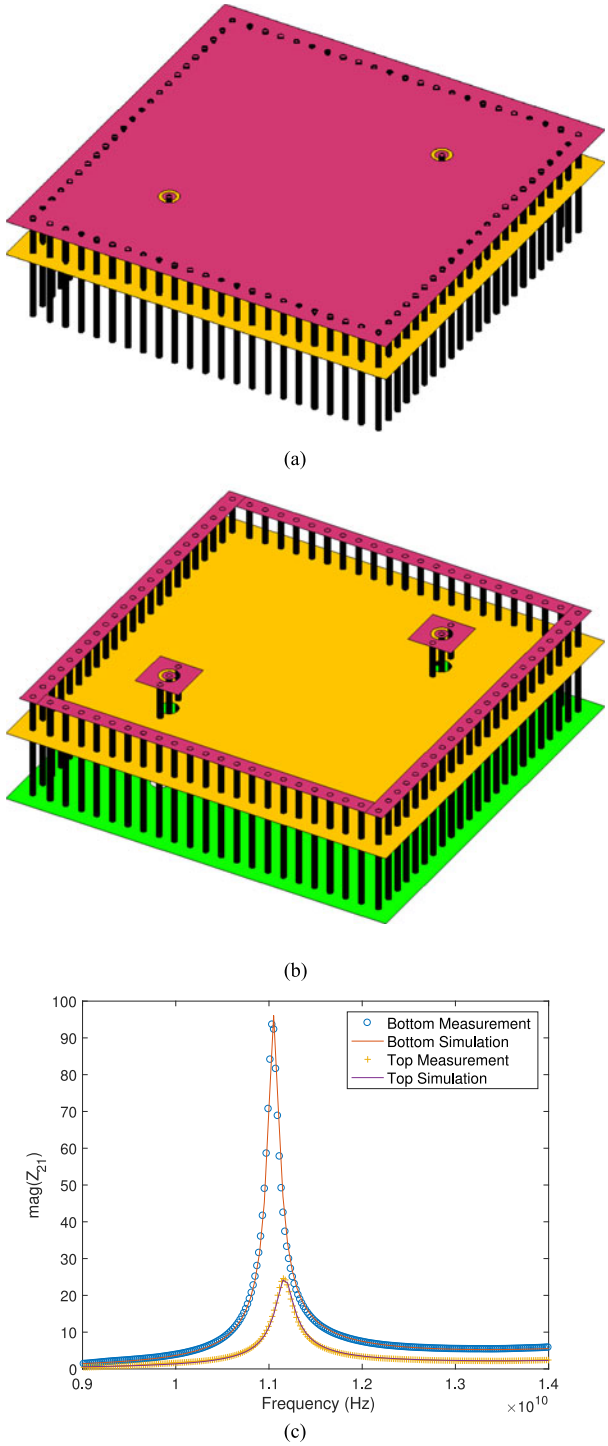

Fig. 7. Shorted cavity resonators used to extract the dielectric thickness, loss tangent, and dielectric thickness. (a) Top substrate. (b) Bottom substrate. (c) Excellent match between simulation and measurement using the extracted parameters.

As expected, the two scattering parameters will be the same for cases where there is no mode conversion (i.e., $S_{dc} = 0$ or $S_{cd} = 0$ as in a symmetrical differential line.) S_{dd}^{p} is obtained from the two-port measurement setup in Fig. 3(b), and has a reference impedance equal to the port impedances in the usual way. As such, there is no need to define modes or mode impedances,

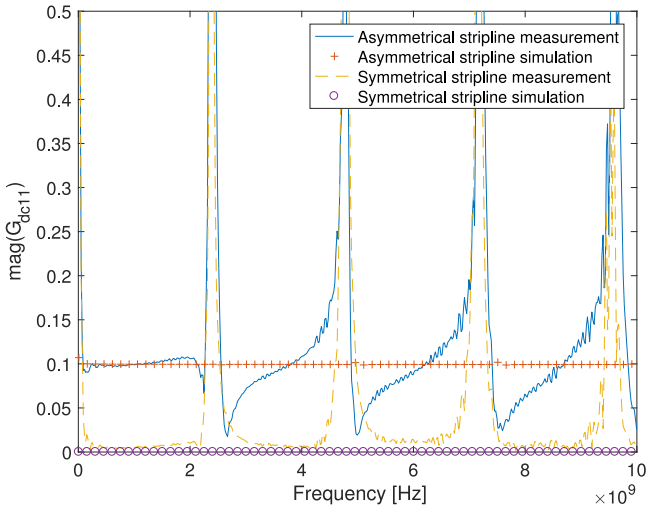

Fig. 8. $G_{dc11} = I_{d1}/I_{c1}$ represents the ratio of differential current to common current. Symmetrical lines will exhibit no mode conversion and have ideally $G_{dc11} = 0$. Simulation agrees well with simulation until the line length approaches 180° at around 2.5 GHz.

resulting in a more intuitive representation of differential circuits compared to traditional mixed-mode scattering parameters. The common-port scattering parameters S^p_{cc} will be extracted from the two-port measurement setup in Fig. 3(a). The mixed-port scattering parameters S^p_{cd} where the left port is the common port is obtained from the measurement in Fig. 4(a). Finally, the measurement setup in Fig. 4(b) would provide S^p_{dc}, where the left port is a differential port.

To provide a comparison between the traditional differential-mode scattering parameters (S_{dd}) and the new differential-port scattering parameters (S^p_{dd}), the same asymmetrical microstrip line example in Fig. 5 has been simulated with Sonnet. Traditional mixed-mode scattering parameters including S_{dd} are calculated from the four-port single-ended scattering parameters. Next, the same microstrip lines are simulated with differential ports in Sonnet. This simulation setup corresponds to the differential-port setup in Fig. 3(b); therefore, it matches the calculated S^p_{dd} from the formula in (24), as shown in Fig. 6. There is a very small discrepancy between calculated S^p_{dd} from formula in (24) and directly simulated S^p_{dd} from Sonnet, which may be due to any differences in deembedding of ports in the simulator.

IV. Simulation to Hardware Correlation

Symmetrical and asymmetrical differential striplines have been characterized using a four-port vector network analyzer. The measured boards consisted of a prepreg as the top substrate of the stripline and a thicker bottom substrate made of MEGTRON6. The nominal thicknesses are 100 μm for the top substrate and 200 μm for the bottom one. The outer conductor layers are 1 oz. copper, whereas the inner layers are 0.5 oz. The nominal dielectric constant is 3.6 and loss tangent is 0.004 at 12 GHz according to the data sheet. To accommodate any deviations from the nominal values, it is important to extract the thickness, dielectric constant, as well as the loss tangent of the dielectrics. We designed simple shorted cavity resonators of

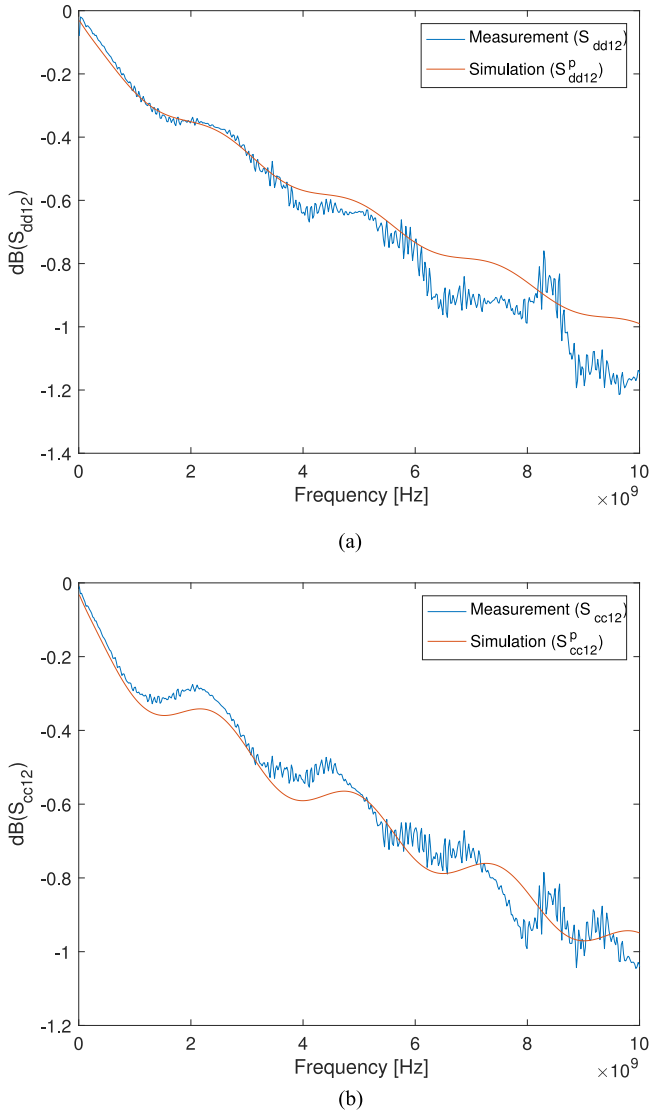

Fig. 9. Measurement to simulation correlation for symmetrical stripline. Mixed-port simulations are obtained using the port configurations in Fig. 3. (a) Differential insertion loss. (b) Common insertion loss.

size 10 mm × 10 mm following the methodology in [20] and [21] as shown in Fig. 7.

The extracted parameters for the top substrate were thickness of 89 μm, dielectric constant of 3.58, and loss tangent of 0.0094. For the bottom substrate, the same parameters were extracted as 211 μm, 3.67, and 0.0069. The higher loss tangent compared to the nominal value can be attributed to the presence of any surface roughness that has not be accounted for during the extraction process. Using the extracted parameters, the shorted cavity resonators were simulated with the full-wave simulator Sonnet [8]. Fig. 7 shows excellent match between the simulation and measurement.

We apply the extracted parameters on the simulation of the striplines using Keysight ADS. The striplines had a length of 3.15 cm. In the symmetrical case, the width and spacing was 100 μm; whereas the width of line 1 was increased to 200 μm for the asymmetrical case. Fig. 8 shows the variation of G_{dc11} as

a function of frequency. An approximately constant differential current to common current ratio is observed as expected. The deviation in measurements from this constant value at around 2.5 GHz can be attributed to the electrical length of the line being close to 180°. This common inaccuracy is observed in, for example TRL calibration, since the scattering parameters of the line standard becomes almost identical to a thru standard around those frequency points [22], and measurement inaccuracies due to the probing pads are amplified.

For symmetrical lines, there is no mode conversion, and the mixed-port scattering parameters are equivalent to the mixed-mode scattering parameters. The measured mixed-mode scattering parameters are compared against simulated mixed-port scattering parameters in Fig. 9. The good agreement indicates the accuracy of the extracted dielectric thickness, loss tangent, and dielectric thickness of the substrate layers. For asymmetrical lines, the new mixed-port parameters would be different than traditional mixed-mode parameters, due to the presence of mode conversion.

V. Conclusion

This paper introduced mixed-port scattering and hybrid parameters for differential circuits. These new parameters are based on simple port definitions, and do not make use of modal quantities such as even, odd, common, or differential-mode impedances. The new hybrid parameters are particularly useful to experimentally characterize the current division factor, a critical parameter for electromagnetic interference analysis of differential lines. The new mixed-port scattering parameters present a promising new way of characterizing and evaluating arbitrary differential circuits, without the ambiguities of existing modified or extended mixed-mode scattering parameter definitions.

References

[1] D. E. Bockelman and W. R. Eisenstadt, "Combined differential and common-mode scattering parameters: theory and simulation," *IEEE Trans. Microw. Theory Techn.*, vol. 43, no. 7, pp. 1530–1539, Jul. 1995.

[2] N. Zhang, K. Kim, H. Lee, and W. Nah, "Theory, simulation, and experiment on extended mixed-mode s-parameters in three-conductor lines," *IEEE Trans. Electromagn. Compat.*, vol. 59, no. 6, pp. 1932–1939, Dec. 2017.

[3] A. Huynh, P. Hakansson, and S. Gong, "Mixed-mode s-parameter conversion for networks with coupled differential signals," in *Proc. Eur. Microw. Conf.*, pp. 238–241, Oct. 2007.

[4] A. Ferrero and M. Pirola, "Generalized mixed-mode s-parameters," *IEEE Trans. Microwa. Theory Techn.*, vol. 54, no. 1, pp. 458–463, Jan. 2006.

[5] T. Rahkonen and J. Kortekangas, "Mixed-mode parameter analysis of fully differential circuits," in *IEEE Int. Symp. Circuits Syst.*, May 2004, vol. 1, pp. I–269–I–272.

[6] H. Erkens and H. Heuermann, "Mixed-mode chain scattering parameters: Theory and verification," *IEEE Trans. Microw. Theory Techn.*, vol. 55, no. 8, pp. 1704–1708, Aug. 2007.

[7] J. Cho *et al.*,"Mixed-mode abcd parameters: Theory and application to signal integrity analysis of pcb-level differential interconnects," *IEEE Trans. Electromagn. Compat.*, vol. 53, no. 3, pp. 814–822, Aug. 2011.

[8] Sonnet v16.52, 2015. [Online]. Available: http://www.sonnetsoftware.com/

[9] H. Tran, L. Barannyk, A. Elshabini, and F. Barlow, "A study of differential signaling: Stable and accurate mixed-mode conversion and extraction of differential s-parameters," in *Proc. IEEE Workshop Microelectron. Electron Devices*, Mar. 2015, pp. 1–4.

[10] S. Huang, "Technique to improve the accuracy of mixed-mode s-parameters derived from single-ended results and application to shorter test coupon design," in *Proc. IEEE Symp. Electromagn. Compat. Signal Integrity*, Mar. 2015, pp. 283–288.

[11] A. E. Engin, I. Ndip, and K. D. Lang, "Mixed-mode hybrid parameters for high-speed differential lines," in *51st Symp. Microelectron.*, Oct. 2018, pp. 1–4.

[12] A. E. Engin, I. Ndip, K. D. Lang, and J. Aguirre, "Differential-line characterization using mixed-port scattering parameters," in *Proc. IEEE MTT-S Int. Conf. Numeric. Electromagn. Multiphys. Model. Optimiz.*, Aug. 2018, pp. 1–3.

[13] Y. Toyota, K. Iokibe, and L. R. Koga, "Mode conversion caused by discontinuity in transmission line: From viewpoint of imbalance factor and modal characteristic impedance," in *IEEE Electr. Des. Adv. Packag. Syst. Symp.*, Dec. 2013, pp. 52–55.

[14] A. E. Engin, W. John, G. Sommer, W. Mathis, and H. Reichl, "Modeling of striplines between a power and a ground plane," *IEEE Trans. Adv. Packag.*, vol. 29, no. 3, pp. 415–426, Aug. 2006.

[15] Advanced Design System, 2016. [Online]. Available: http://www.keysight.com

[16] G. A. Matig-a, M. R. Yuce, and J. M. Redout, "An integrated LVDS transmitter-receiver system with increased self-immunity to EMI in 0.18-μm CMOS," *IEEE Trans. Electromagn. Compatib.*, vol. 58, no. 1, pp. 231–240, Feb. 2016.

[17] "Ieee standard for low-voltage differential signals (LVDS) for scalable coherent interface (sci)," *IEEE Std 1596.3-1996*.

[18] D. Kim, H. Kim, and Y. Eo, "Efficient eye diagram determination of strongly coupled lines for differential signals," in *Proc. Int. SoC. Des. Conf.*, pp. 221–224, Nov. 2010.

[19] J. Cho, E. Song, J. Shim, Y. Shim, and J. Kim, "A fast and precise eye-diagram estimation method for a channel of a pair of differential microstrip lines on pcb with arbitrary terminations," in *IEEE Electr. Des. Adv. Packag. Syst. Symp.*, Dec. 2009, pp. 1–4.

[20] A. E. Engin, "Extraction of dielectric constant and loss tangent using new rapid plane solver and analytical debye modeling for printed circuit boards," *IEEE Trans. Microw. Theory Techn.*, vol. 58, no. 1, pp. 211–219, Jan. 2010.

[21] A. E. Engin and P. Pasunoori, "Automated complex permittivity characterization of ceramic substrates considering surface-roughness loss," *J. Microelectron. Electron. Packag.*, vol. 9, pp. 144–148, 2012.

[22] B. Hofmann and S. Kolb, "A multistandard method of network analyzer self-calibration-generalization of multiline TRL," *IEEE Trans. Microw. Theory Techn.*, vol. 66, no. 1, pp. 245–254, Jan. 2018.

Arif Ege Engin (M'05) received the B.S. and M.S. degrees in electrical engineering from Middle East Technical University, Ankara, Turkey, and from University of Paderborn, Germany in 1998 and 2001, respectively. He received the Ph.D. degree from the University of Hannover, Hanover, Germany in 2004.

He worked as a Research Engineer with the Fraunhofer-Institute for Reliability and Microintegration in Berlin, Germany. From 2006 to 2008, he was an Assistant Research Director of the Microsystems Packaging Research Center, Georgia Tech. He is currently an Associate Professor with the Department of Electrical and Computer Engineering, San Diego State University, San Diego, CA, USA. He has authored and coauthored more than 100 journals and conferences in the areas of signal and power integrity modeling and simulation and four patents. He is the Co-author of the book "*Power Integrity Modeling and Design for Semiconductors and Systems*," translated to Japanese and Chinese.

Dr. Engin is the recipient of the Semiconductor Research Corporation Inventor Recognition Award in 2009, Outstanding Educator Award from the International Microelectronics Packaging and Assembly Society in 2015, the Alexander-von-Humboldt Research Fellowship for 2015–2018, and 2017 IEEE EMC-S M. Kanda Award for the most cited paper in the last 5 years (2013–2017).

Ivan Ndip (M'05–SM'12) received the M.Sc. and Ph.D. degrees with the highest distinction (*summa cum laude*) from the Technical University Berlin, Berlin, Germany, in 2002 and 2006, respectively, all in electrical engineering.

He joined the Fraunhofer-Institute for Reliability and Microintegration (IZM), Berlin, as a Research Engineer in 2002. In June 2005, he was appointed as the Group Manager of RF Modeling and Simulation. Six months later, he established the RF & High-Speed System Design Group at IZM, and served as the Founding Group Manager until June 2015. From 2005 to 2015, he built-up and led a dynamic team of Research Engineers and Scientists. During this period of 10 years, he led fundamental research projects, and industrial R&D projects, with national and international partners in the areas of measurement and analysis of dielectric materials in dependency on frequency and temperature; electromagnetic modeling, numerical simulation, measurement and optimization of integrated antennas; high-frequency characterization and optimization of RF components, modules and systems for signal/power integrity and intra-system EMC; design of power-distribution networks and suppression of power-ground noise in mixed-signal modules, and RF system-integration of transceiver modules. Since January 2014, he has been the head of the Department of RF & Smart Sensor Systems at IZM. He has been a Lecturer in the School of Electrical Engineering and Computer Sciences at TU Berlin since 2008. He also teaches Professional Development Courses to practicing Engineers and Scientists worldwide. He has authored and coauthored more than 150 publications in referred journals and conference proceedings.

Dr. Ndip is a recipient of six Best Paper Awards at leading international conferences as well as a recipient of the Tiburtius-Prize, awarded yearly for outstanding Ph.D. dissertations in the State of Berlin, Germany. He is also the recipient of the 2012 Fraunhofer IZM Research Award for his work on the development and successful application of novel Methods, Models and Design Measures for Electromagnetic Optimization of High-frequency and High-speed Systems, and the recipient of the 2016 John A. Wagnon Technical Achievement Award for his outstanding technical contributions to the microelectronics industry worldwide. He chairs the Signal & Power Integrity Committee of the International Microelectronics Assembly and Packaging Society (IMAPS). He is an Associate Editor of the Journal of Microelectronics and Electronic Packaging. He is also a reviewer of IEEE Transactions on EMC, CPMT, MTT, ED, and other international Journals. He is a member of the Technical Program Committee of many IEEE and IMAPS international conferences. He was a Technical Co-Chair of the 44th and 45th International Symposiums on Microelectronics in Long Beach, and San Diego, CA, USA, in 2011 and 2012, respectively. In 2013, he was the Technical Chair of the 46th International Symposium on Microelectronics in Orlando, FL, USA, and in 2014 he became the General Chair of the 47th International Symposium on Microelectronics, in San Diego, CA, USA. He also served as the General Chair of the 19th IEEE Workshop on Signal and Power Integrity (SPI 2015), in Berlin, Germany. He is a Fellow, and Life Member of IMAPS.

Klaus-Dieter Lang (M'08–SM'13) received the M.Sc. (Dipl.-Ing.) degree in electrical engineering from Humboldt University (HU), Berlin, Germany, in 1981, and two doctorate degrees (on wire bonding of multilayers and on quality assurance in assembly processes) from HU, in 1985 and 1989, respectively.

In 1981, he joined the Humboldt University as a Researcher, where he was engaged in microelectronic assembly, packaging, and quality assurance up till 1991. In 1991, he joined SLV Hannover to build up a department for microelectronic and optic components manufacturing. In 1993, he became the Department Manager for Chip Interconnections, Fraunhofer Institute for Reliability and Microintegration (IZM), Berlin, where he was the Directors Personal Assistant from 1995 to 2000, and also responsible for Marketing and Public Relations. From 2001 to 2005, he coordinated the Branch Lab Microsystem Engineering, Adlershof, Berlin. From 2003 to 2005, he was the Head of the Department Photonic and Power System Assembly and from 2006 to 2010; he has been the Deputy Director of IZM. Since 2011, he has been the director of Fraunhofer IZM and a Professor at the Technical University Berlin. He is the author or coauthor of three books and more than 130 publications in the field of wire bonding, microelectronic packaging, microsystems technologies, and chip on board.

Prof. Lang is Member of numerous scientific boards and conference committees, which include the Semiconductor Equipment and Materials International Award Committee, the Scientific Advisory Board of European Cluster of Electronic Packaging and Integration of Microdevices and Smart Systems, the Executive Board of VDE-GMM, and the Scientific Chair of the Conference Technologies of Printed Circuit Boards and SMT/HYBRID/PACKAGING. He is a Member of the Deutscher Verband fr Schweien und verwandte Verfahren eV (DVS), and International Microelectronic Assembly and Packaging Society, and plays an active role in the international packaging community as well as in conference organization.

Gerardo (Jerry) Aguirre (M'96–SM'14) was born in El Paso, Tx, in 1960. He received the B.S. degree in electrical engineering from the University of Texas at El Paso, El Paso, TX, USA, in 1983, and the M.S. and Ph.D. degrees in electrical engineering from the University of Arizona, in 1986 and 1996, respectively.

He was with Antenna Development Division, Radar Department, Sandia Laboratories, the Atmospheric Sciences Division, Los Alamos National Laboratories, and the electronics package group at Texas Instruments. He is currently a Member of the Technical Staff with the Product Technology Center at Kyocera International, San Diego, CA, USA. His research interests include electrical performance of electronic packages and high frequency properties of integrated circuit packages.